Instantaneous spectral attributes associated to LNAPL phases

Luis. A. Peche[1], Jandyr. M. Travassos[1],
1-Observatório Nacional, Rio de Janeiro, RJ, Brazil

Abstract

Instantaneous spectral analysis applied on 7 CMP profiles is used to detect some of the few phases developed from a young controlled spill of 100 l of LNAPL. The presence of the LNAPL affects the traces differently at earlier and later times and introduces important spectral changes. The LNAPL concentrates the spectral energy within a window in the time-frequency spectrum, bounded in frequency and in TWT. Below the TWT range amplitudes are attenuated producing a low frequency shadow zone below it. The late TWT bound not only limits the useful time information in the trace but also is very sensitive to the vapor phase of the LNAPL. We use this bound as a useful instantaneous attribute of the GPR trace. The LNAPL also narrows and attenuates the amplitudes inside the spectral window, acting as a filter for the scattered field from a volume limited in depth by the late TWT bound. We suggest the construction of a spectral pseudo-section, which is able to show clearly the limits of the influence of the LNAPL.

Keywords - GPR imaging; instantaneous spectral analysis; hydrocarbon contamination; LNAPL; controlled spill; wavelet transform.

Introduction

GPR has become prevalent amongst other geophysical methods in assessing contaminated sites, as it is a fast and reliable tool to image the subsurface. But to detect LNAPLs directly from GPR sections may prove to be a difficult task as the free-phase LNAPL and the background medium usually have dielectric properties that are not so distinct as to provide enough reflectivity coefficient contrast to stand itself out in a GPR section. On the other hand as the contaminant ages the electrical conductivity of the dissolved phase may experiment a conspicuous increase as a result of a ionic build up from its natural biodegradation making easier to map the extension of the plume and by the same token obliterating the information below it. An alternative approach may be to use radar imagery to construct a model the geologic structure of the subsurface thus providing a starting point for a hydrogeologic model capable of predicting the fate and transport of contaminants. A more ambitious task would be to extend the model to assign estimates of hydrogeologic parameters like water content, porosity and permeability, to quantitative model the long-term transport of the contaminant.

The dielectric properties at a multicomponent LNAPL spill scenario are determined by the volume fractions and dielectric constants of the individual components (Knight, 2001; Topp et al., 1980). One rigorous approach to this class of problem is to use of an effective medium theory (EMT) that incorporate effects such as the geometry of the components in predicting dielectric properties (Knight, 2001). When more than one fluid is present the effect of the interaction of solid-fluid but also the fluid-fluid phases must be considered (Endres & Redman, 1996).

This paper presents a procedure for detecting the LNAPL spectral signature in a fresh controlled spill of gasoline in an open experiment. The approach presented here is to use an instantaneous spectral decomposition procedure that can provide a time-frequency analysis of the trace, thus revealing the time-dependent frequency response of the subsurface. Instantaneous spectral decomposition is currently used in seismic to characterize the time-dependent frequency response of reservoir rocks.

Instantaneous Spectral Decomposition Analysis

Spectral decomposition methods such as short-window discrete Fourier transform (SWDFT), wavelet transform (WT) and Matching Pursuit Decomposition (Mallat et al, 1993) have been extensively used for spectral decomposition of seismic data with the goal of estimating tuning thickness, mapping stratigraphic variability and as direct hydrocarbon indicators (Castagna et al., 2003; Sinha et al., 2005). Spectral analysis has also been applied to GPR data to analyze the spatial variation of the signal spectral attenuation over a crude oil spill using the discrete Fourier transform (DFT) (Burton et al., 2004) or to recognize the affected spectral components over a gasoline spill (Peche & Travassos, 2006) using the wavelet packet decomposition (WPD) technique (Coifman et al., 1992).

The instantaneous spectral analysis (ISA) is a continuous time-frequency analysis technique that can provide a frequency spectrum for given time samples of a GPR trace. The ISA can be done with both SWDFT and WT with varying resolution in both time and frequency. The analyzing window length is fixed for SWDFT whereas the WT uses a variable length, which is inversely proportional

to the frequency being analyzed. With the WT we can avoid the need to choose the SWDFT window length.
We use the continuous wavelet transform (CWT) to represent the trace through dilations and translations of a complex B-Spline mother wavelet.

To perform the ISA we transform the continuous wavelet transform scalogram into a time-frequency spectrum TFCWT (Sinha et al., 2005) $W(f,t)$ to obtain the instantaneous spectral attributes of the GPR trace: center frequency, dominant frequency and spectral bandwidth. Those attributes are defined as moments of the TFCWT (Sinha et al., 2005) as follows.

The instantaneous center frequency can be estimated by

$$f_c(t) = \frac{\int_0^\infty f\,|W(f,t)|^2\,df}{\int_0^\infty |W(f,t)|^2\,df} \qquad (1)$$

where f, t represent the frequency and time, respectively. The bandwidth can be estimated by

$$f_{bw}(t) = \frac{\int_0^\infty (f-f_c)^2\,|W(f,t)|^2\,df}{\int_0^\infty |W(f,t)|^2\,df} \qquad (2)$$

With relations (1) and (2) we define an upper and a lower limit to $f_c(t)$ as

$$f_{\pm}(t) = f_c(t) \pm \frac{1}{2} f_{bw}(t) \qquad (3)$$

The Controlled Spill and Fieldwork

This work uses a GPR data set collected over a controlled spill of 100 l of Brazilian gasoline having 24 % ethanol. The spill was part of a geochemistry experiment carried out in a research farmland, southeastern Brazil. The local geology is characterized by unconsolidated deposits of eolian, alluvial, lacustrine and marine sands with less than 5 % of silt and clay. The soil has a hydraulic conductivity of 10-4 cm/s, an effective porosity of 0.20 and a groundwater flow of 2.8 m/yr (Corseuil et al, 2000), with the depth to the seasonal water table 2 m.

A first geochemical campaign one month after the spill detected ethanol and BTEX compounds only at well A, right at the center of the hole (Figure 1). A second geochemical campaign two months after the spill detected ethanol and BTEX compounds only at wells A and C (Figure 1). The geophysical fieldwork occurred in between these two geochemical campaigns. At that time we were able to smell gasoline vapors in nine of the monitoring wells, situated inside the dashed green perimeter shown in Figure 1. This indicates that although a free or dissolved phase may have migrated some more than 1 m towards the SE in three months, a sizable vapor phase developed on an area more than 3 m in diameter, centered at the hole.

This work deals with the data from 7 CMP profiles running SW-NE, all 9 m long with a minimum offset of 0.6 m, numbered 7 to 13 in Figure 1. We have used a Pulse Ekko 100 with 200 MHz antennae, 400 ps sampling rate, 32 stack and 0.1 m spatial sampling. We kept the Antennae in a broadside-perpendicular configuration, with stop-and-go firing assuring the best antenna coupling with ground surface.

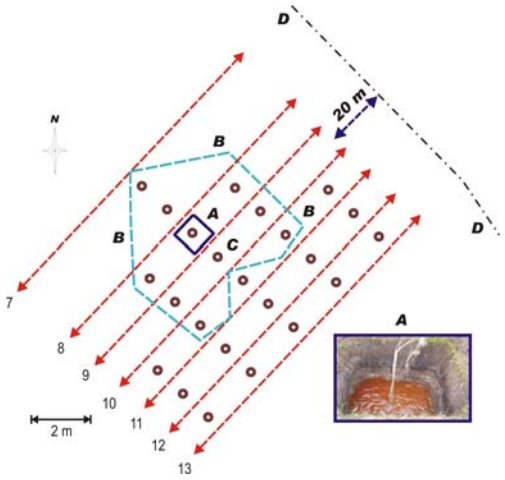

Figure 1. *Schematic map of the study area containing the elements referred to in the text. Seven CMP profiles, 9 m in length each, run along the NE - SW (dashed red lines) direction, numbered 7 to 13. The gasoline was poured into a hole shown as a blue square marked A. The monitoring wells are shown as open magenta circles. The dashed turquoise perimeter surrounds the wells where we found organoleptic evidence of the vapor phase. The free phase was detected only in two wells, one at the center of the hole A and at C. The inset A shows the hole being filled with gasoline, showing the supporting structure of a monitoring well at its center. The dot-dashed line D is a metallic fence (distance not to scale).*

Results

The processing flow included dewow, SEC gain, band-pass filter (15, 20, 300, 310 MHz), dip filter, NMO correction and stack. The attenuation factor used in the gain to account for the wavefront spherical spreading and exponential decay was estimated by the exponential decay of the average envelope of a fixed-offset profile coincident with CMP 9 (Figure 1). We assume the offset-dependent changes in amplitude caused by the radiation pattern of the antennas approximately uniform for all profiles. The dip filter was used to eliminate the artifacts caused by a metallic fence 20 m away from the NE limit of

the studied area (Figure 1). After stack the NMO corrected CMP's produced 7 stacked traces, located approximately at the center of each CMP profile shown in Figure 1 and therefore 1 m apart form each other but traces 7 and 8 that are 2 m apart. Semblance analysis reveals a two-velocity model with 0.09 – 0.12 m/ns down to 1 m on top of lower velocities around 0.07 m/ns.

Taking into consideration Figure 1 together with the geochemical and organoleptic data we can assume that profile 10 is under the direct influence of all the LNAPL phases: free, dissolved and vapor. By the same token profile 13 is the least influenced of all due to its distance from the spill hole, we may assume it is beyond the reach of any of the phases of the contaminant. All other profiles are more or less influenced by the vapor phase. Obviously we are considering that the GPR trace carries information not only from what is situated directly below a given measuring point but also laterally. From now on we are going to use the CMP profile number to refer to the stacked traces, i.e., the stacked trace of CMP 10 is referred to as trace 10.

A comparison between traces 10 and 13 indicates that the presence of the LNAPL affects the traces at both earlier and later times (Figure 2). Important phase differences are seen for TWT $\leq$ 60 ns, corresponding to depths just below the bottom of the hole and above the water table, and a decrease in amplitude for TWT > 130 ns. The correlation between the two traces TWT $\leq$ 60 ns, estimated using windows of 9.6 ns with 50% overlap falls in the range [-.75, -.5]. We speculate here those changes are a result of the observed spectral changes, and consequently in pulse wavelength. Trace 10 shows a decrease in reflectivity over the contaminated area above and the water table probably due the LNAPL giving rise to a gradient in soil dielectric properties that smear out the variation in permittivity (Burton et al., 2004). The spectrum of trace 10 is less energetic and narrower than the corresponding of trace 13. The main energy of trace 10 is distributed in a spectral band of 110 - 140 MHz, 27 % shorter than of the corresponding band of trace 13 over 60 - 150 MHz (Figure 2). All this together indicates that some of the observed spectral changes may be due to changes in trace 10, restricted to a given time interval. The need to identify that time interval and, maybe, also its relative importance to the observed spectral changes suggest the need to perform an ISA in our data.

We do the ISA calculating the continuous WT of each trace using a complex B-Spline mother wavelet. With the TFCWT spectrum we can estimate the instantaneous spectral attributes of a given trace, center frequency and the spectral bandwidth, using relations (1) and (2). Figure 3 shows the time-frequency spectrum for trace 10 together with its attributes.

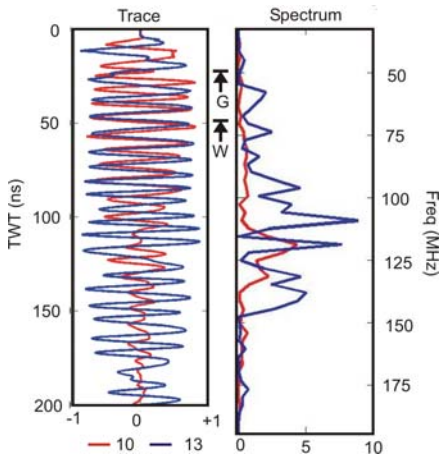

Figure 2. *The left panel shows the stacked traces of profiles 10 (red) and 13 (blue), normalized to their maxima. The right panel shows the spectra of the two traces with the same color convention. G and W indicate the bottom of the spill hole and the water level, respectively.*

Most of the spectral energy of trace 10 is concentrated in a window in the TFCWT spectrum limited by frequencies 100 and 150 MHz and TWT's 30 and 100 ns. Those TWT limits correspond to a volume with the maximum depth shorter than 4 m. This indicates that the LNAPL filters out frequencies outside a given time-frequency window, almost as if it shone back a color from a depth range. Below the TWT range of the window, trace amplitudes are attenuated. Note that this attenuation cannot be explained by any increased electrical conductivity of a biodegraded dissolved phase as we are dealing with a young spill.

The time-frequency spectra for all the 7 stacked traces are put together as a spectral pseudo-section in Figure 3, with the spectral bandwidth limits and the break down point of the center frequency defining each trace's useful spectral window. We use a least-squares polynomial fit to the break points as the later time limit of the spectral pseudo-section.

Figure 3 shows that the LNAPL shortens and narrows the spectral windows, concentrating the spectral information to earlier times and to a shorter frequency range. The latter was also seen in the trace amplitude spectrum of trace 10 shown in Figure 2. Only traces 8 and 9, and maybe 10 are under the direct influence of all phases of the LNAPL. Considering this fact we may conclude the vapor phase that by the organopleptic evidences developed in volume at least from trace 7 to trace 11 plays a major role in affecting the spectral contents of traces. We may even say that the vapor phase affects even trace 12, probably as a minor lateral, NW, influence. Break points occur at traces 9 and 10 at the earliest

times. The shortening of spectral windows is conspicuously correlated with the reach of the LNAPL. It is also evident from Figure 3 that the LNAPL obviously lowers the total spectral energy of the affected traces, but the amplitude maxima are somewhat preserved albeit in a shorter window, allowing the idea the LNAPL shines back a, say, color spot.

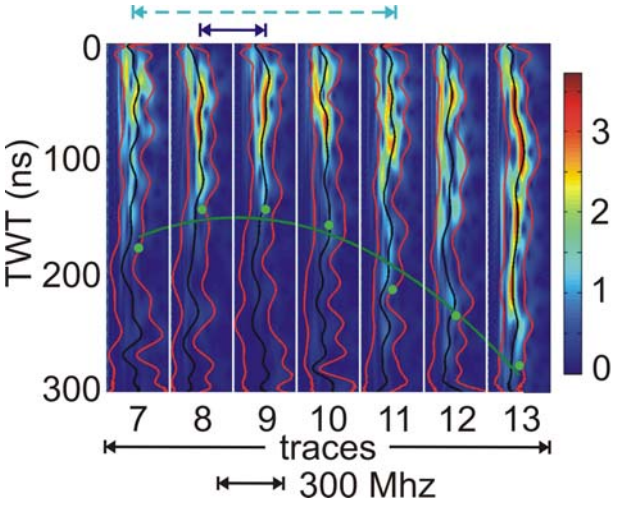

Figure 3. *Time-frequency spectrum panels for the 7 stacked traces put together as a pseudo-section. All traces are 1 m apart from its immediate neighbors but traces 7 and 8 that are 2 m apart. The color bar indicates the normalized spectral amplitude. The frequency axis is horizontal, the scale is shown at the bottom. The smoothed center frequency is shown as a black line. The spectral bandwidth limits are shown with two red lines. The green dots at half-width of each panel mark the numerical stability break down point of the center frequency for each trace. The green line is a least-squares polynomial fit to the green dots and serves as the later time limit of the spectral pseudo-section. The spill hole relative location is shown at the top as a blue double arrow. The dashed turquoise double arrow shows the range of the organoleptic evidence of the vapor phase.*

Conclusions

The LNAPL concentrates the spectral energy within a window in the TFCWT spectrum with bounds in frequency and in TWT. Below the TWT range of the window trace amplitudes are attenuated producing a shadow zone below it. This attenuation cannot be explained by any enhancement in electrical conductivity of a biodegraded dissolved phase as we are dealing with a young spill. The late time boundary of the spectral window can be estimated to be at the TWT where the rms of the center frequency becomes larger than the spectral bandwidth, two instantaneous attributes of the trace. That TWT coincides with the point where the numerical stability of the center frequency estimator breaks down and the amplitude falls to –20 Db of the spectral maximum. This break point limits the useful information in the trace in time and is very sensitive to the vapor phase of the LNAPL and in thus can be considered as a useful instantaneous attribute itself. The LNAPL also narrows and attenuates the amplitudes inside the spectral window, in other words filtering out frequencies almost as if it shone back a color from a volume limited in depth by the TWT corresponding to the break point and the velocity of the medium.

Acknowledgements

The fieldwork was entirely funded by Petrobras. The authors thank Petrobras for the permission to present the results and to UFSC for the permission to do the fieldwork in their test site. JT is a recipient of a research scholarship from CNPq.

References

Burton, B.L., Olhoeft, G. R., and M.H. Powers, 2004, Frequency spectral analysis of GPR data over a crude oil spill: Tenth International Conference on Ground Penetrating Radar.

Castagna, J.P., Sun, S., and Siegfried, R.W., 2003, Instantaneous spectral analysis: Detection of low-frequency shadows associated with hydrocarbons, The Leading Edge, 22, 120-127.

Coifman , R.R., and Wickerhauser, M.V., 1992, Entropy-based algorithms for best basis selection, IEEE Trans. Inform. Th., 38, 713-719.

Corseuil, H.X., Fernandes, M., Rosário, M., and P.N. Seabra, 2000, Results of a Natural Attenuation Field Experiment for an Ethanol-Blended Gasoline Spill, In: Proceedings of the Petroleum Hydrocarbons and Organic Chemicals in Ground Water: Prevention, Detection, and Remediation, 24-31.

Endres A.L., and Redman J.D. 1996, Modeling the electrical properties of porous rocks and soils containing immiscible contaminants, J. Environ. Eng. Geophys., 1, 88–96.

Knight, R., 2001, Ground penetrating radar for environmental applications, Ann. Rev. Earth Planet. Sci.. 29, 229–55.

Mallat, S., and A. Zhang, 1993, Matching pursuit with time frequency dictionaries, IEEE Trans. Signal prec., **41**, 3397-3415.

Peche, L.A., and Travassos, J.M., 2006, Direct detection of contamination using GPR, II Simpósio Brasileiro de Geofísica, Natal, Brasil, Extended Abstract (070) in CD ROM: 4p.

Sinha, S., Routh, P.S., Anno, P.D., and J.P. Castagna, 2005, Spectral decomposition of seismic data with continuous-wavelet transform: Geophysics, **70**: 19-25.

Topp G.C., Davis J.L., and Annan A.P., 1980, Electromagnetic determination of soil water content: measurement in coaxial transmission lines, Water Resour. Res., 16, 574–82.